Available online at www.sciencedirect.com

ScienceDirect

ELSEVIER

International Journal of Solids and Structures 44 (2007) 4472–4491

INTERNATIONAL JOURNAL OF SOLIDS and STRUCTURES

www.elsevier.com/locate/ijsolstr

Intensity of singular stress fields causing interfacial debonding at the end of a fiber under pullout force and transverse tension

Nao-Aki Noda *, Ryohji Shirao, Jun Li, Jun-Suke Sugimoto

Mechanical Engineering Department, Kyushu Institute of Technology, 1-1, Sensui-cho, Tobata, Kitakyushu 804-8550, Japan

Received 7 July 2006; received in revised form 30 October 2006
Available online 1 December 2006

Abstract

In this study, singular stress fields at the ends of fibers are discussed by the use of models of rectangular and cylindrical inclusions in a semi-infinite body under pullout force. Those singular stresses have not been discussed yet in the previous studies for pullout problems although they are important for causing interfacial initial debonding. The body force method is used to formulate those problems as a system of singular integral equations where unknowns are densities of the body forces distributed in a semi-infinite body having the same elastic constants as those of the matrix and inclusions. In order to compare the results with the previous solutions, tension problems of a fiber in a semi-infinite body are also considered. Then, generalized stress intensity factors at the corner of rectangular and cylindrical inclusions are systematically calculated for various geometrical conditions with varying the elastic ratio, length, and spacing of the location from edge to inner of the body. The effects of elastic modulus ratio and aspect ratio of inclusion upon the stress intensity factors are discussed for pullout problems.

Keywords: Elasticity; Composite material; Fracture mechanics; Body force method; Singular integral equation; Generalized stress intensity factor; Cylindrical inclusion

1. Introduction

In short-fiber-reinforced composites, fibers are mainly used to enhance load carrying capacity by reducing stresses and strains in matrix. However, singular stress appearing at the fiber ends causes crack initiation, crack propagation, and final failure under cyclic loading (Nisitani et al., 1993). To evaluate the mechanical strength of these composites, therefore, it is necessary to know the intensity of those singular stresses. In our previous studies, we have discussed the intensities at the fiber including periodic and zigzag arrays of fibers (Noda and Takase, 2003, 2005).

Fibers are also used for fracture toughness enhancement. In this aspect, the interaction of a fiber with the matrix in which it is embedded is of great interest. In the previous studies, load transfer from

* Corresponding author. Tel./fax: +81 93 884 3124.
E-mail address: noda@mech.kyutech.ac.jp (N.-A. Noda).

0020-7683/$ - see front matter
doi:10.1016/j.ijsolstr.2006.11.034

Notations

l_x, l_y	dimensions of rectangular inclusion
l_r, l_z	dimensions of cylindrical inclusion
G_M,G_I	shear modulus for matrix and inclusion
ν_M, ν_I	Poisson's ratio for matrix and inclusion
G_1, G_2	shear modulus of bonded strip for materials 1 and 2
ν_1, ν_2	Poisson's ratio of bonded strip for materials 1 and 2
P	magnitude of pull-out force
α, β	Dundurs parameter $\left[\alpha = \frac{G_M(\kappa_I+1)-G_I(\kappa_M+1)}{G_M(\kappa_I+1)+G_I(\kappa_M+1)},\ \beta = \frac{G_M(\kappa_I-1)-G_I(\kappa_M-1)}{G_M(\kappa_I+1)+G_I(\kappa_M+1)}\right]$
λ_1	singular index for mode I at corner A
λ_2	singular index for mode II at corner A
λ	singular index at corner B
$\sigma_{ij,k}$	singular stress field at the corner k
$\tau_{ij,k}$	singular stress field at the corner k
σ_x^∞	stress at infinity
K_{I,λ_1}	generalized stress intensity factor for mode I at corner A
$K_{\mathrm{II},\lambda_2}$	generalized stress intensity factor for mode II at corner A
K	generalized stress intensity factor at corner B
$f^{\mathrm{I}}_{ij,k}, f^{\mathrm{II}}_{ij,k}$	functions for singular stress at corner A
$f_{ij,k}$	functions for singular stress at corner B
F_{nM}, F_{tM}, F_{nI}, F_{tI}	body forces densities
$h^{F_{nM}}_{nn}$, $h^{F_{tM}}_{nn}$, $h^{F_{nI}}_{nn}$, $h^{F_{tI}}_{nn}$	normal stress σ_n in a semi-infinite body induced by a point force F_{nM}, F_{tM}, F_{nI}, F_{tI}
W^{I}_{nM}, W^{I}_{tM}, W^{I}_{nI}, W^{I}_{tI}, W^{II}_{nM}, W^{II}_{tM}, W^{II}_{nI}, W^{II}_{tI}	weight functions
$r_1^{\lambda_1-1}$, $r_1^{\lambda_2-1}$	fundamental densities to express singular stress
a_n, b_n, c_n, d_n, e_n, f_n, g_n, h_n	unknown coefficient

a rod to a surrounding elastic material was originally reported in (Muki and Sternberg, 1969, 1970; Luk and Keer, 1979). Experiment on fiber debonding and pullout was studied in detail, for example, in Cook et al. (1989). Fiber pullout was simulated in terms of a boundary value problem with a finite element method for a circular cylinder with a rigid fiber embedded in its center (Atkinson et al., 1982; Freund, 1992; Povirk and Needleman, 1993). Interfacial debonding and frictional sliding associated with the fiber pullout process are two important mechanisms to increase the toughness; and therefore, recent analyses have focused on these mechanisms assuming the bridging law for a cracking in the wake region (Budiansky et al., 1995; Zhang et al., 2004). However, singular stress appearing at the fiber ends has not been discussed yet in those previous papers although they may cause interfacial initial debonding.

In this paper, fiber pullout is modeled as rectangular and cylindrical inclusions in semi-infinite bodies. Then, the body force method will be used to formulate the problems as a system of singular integral equations. In order to compare the results with the previous solution, tensions of a semi-infinite plate with a fiber and a bonded strip will be also considered. The boundaries will be divided into several intervals, and at each interval unknown body force densities will be approximated accurately by using fundamental densities and power series. Here, the fundamental densities will be chosen to express the singular stress fields exactly (Noda and Takase, 2003, 2005). And finally, the intensity of singular stress at the interface edge points will be discussed with varying aspect ratio and elastic modulus ratio of fibers.

2. Generalized stress intensity factors at the corners of fiber ends

In this paper, rectangular and cylindrical inclusions are considered as models of fibers as shown in Fig. 1(a) and (b).

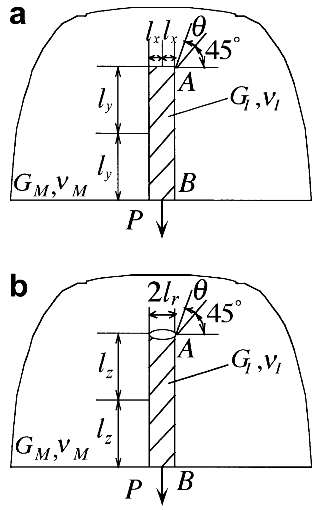

Fig. 1. (a) A rectangular inclusion (b) a cylindrical inclusion in a semi-infinite plate (body) under pull out force.

On the one hand, singular stress around the corner A can be expressed as follows:

$$\sigma_{ij,\mathrm{k}} = \frac{K_{\mathrm{I},\lambda_1}}{r^{1-\lambda_1}} f^{I}_{ij,k} + \frac{K_{\mathrm{II},\lambda_2}}{r^{1-\lambda_2}} f^{\mathrm{II}}_{ij,k} \qquad (ij = r,\, \theta,\, r\theta; \quad k = M, I) \tag{1}$$

For matrix M $(-3\pi/4 \leqslant \theta \leqslant 3\pi/4)$,

$$\left.\begin{aligned}
f^{\mathrm{I}}_{\theta,M}(\theta) &= \tfrac{\lambda_1}{\sqrt{2\pi}(\alpha-\beta)} \langle [-\lambda_1(\alpha-\beta)\cos(\lambda_1\pi/2) + (1-\beta)\sin(\lambda_1\pi)] \times \cos\{(\lambda_1+1)\theta\} \\
&\quad + [(\lambda_1+1)(\alpha-\beta)\sin(\lambda_1\pi/2)] \times \cos\{(\lambda_1-1)\theta\}\rangle \\
f^{\mathrm{II}}_{\theta,M}(\theta) &= \tfrac{\lambda_2}{\sqrt{2\pi}(\alpha-\beta)} \langle [-\lambda_2(\alpha-\beta)\cos(\lambda_2\pi/2) - (1-\beta)\sin(\lambda_2\pi)] \times \sin\{(\lambda_2+1)\theta\} \\
&\quad + [(\lambda_2+1)(\alpha-\beta)\sin(\lambda_2\pi/2)] \times \sin\{(\lambda_2-1)\theta\}\rangle \\
f^{\mathrm{I}}_{r\theta,M}(\theta) &= \tfrac{\lambda_1}{\sqrt{2\pi}(\alpha-\beta)} \langle [-\lambda_1(\alpha-\beta)\cos(\lambda_1\pi/2) + (1-\beta)\sin(\lambda_1\pi)] \times \sin\{(\lambda_1+1)\theta\} \\
&\quad + [(\lambda_1-1)(\alpha-\beta)\sin(\lambda_1\pi/2)] \times \sin\{(\lambda_1-1)\theta\}\rangle \\
f^{\mathrm{II}}_{r\theta,M}(\theta) &= \tfrac{-\lambda_2}{\sqrt{2\pi}(\alpha-\beta)} \langle [-\lambda_2(\alpha-\beta)\cos(\lambda_2\pi/2) - (1-\beta)\sin(\lambda_2\pi)] \times \cos\{(\lambda_2+1)\theta\} \\
&\quad + [(\lambda_2-1)(\alpha-\beta)\sin(\lambda_2\pi/2)] \times \cos\{(\lambda_2-1)\theta\}\rangle
\end{aligned}\right\} \tag{2a}$$

For inclusion I $(-\pi \leqslant \theta \leqslant -3\pi/4,\ 3\pi/4 \leqslant \theta \leqslant \pi)$,

$$\left.\begin{aligned}
f^{\mathrm{I}}_{\theta,\mathrm{I}}(\theta) &= \tfrac{-C_1\lambda_1}{\sqrt{2\pi}(\alpha-\beta)} \langle [-\lambda_1(\alpha-\beta)\cos(\lambda_1\pi/2) + (1+\beta)\sin(\lambda_1\pi)] \times \cos\{(\lambda_1+1)(\pi-\theta)\} \\
&\quad + [(\lambda_1-1)(\alpha-\beta)\sin(\lambda_1\pi/2)] \times \cos\{(\lambda_1-1)(\pi-\theta)\}\rangle \\
f^{\mathrm{II}}_{\theta,\mathrm{I}}(\theta) &= \tfrac{C_2\lambda_2}{\sqrt{2\pi}(\alpha-\beta)} \langle [-\lambda_2(\alpha-\beta)\cos(\lambda_2\pi/2) - (1+\beta)\sin(\lambda_2\pi)] \times \sin\{(\lambda_2+1)(\pi-\theta)\} \\
&\quad + [(\lambda_2+1)(\alpha-\beta)\sin(\lambda_2\pi/2)] \times \sin\{(\lambda_2-1)(\pi-\theta)\}\rangle \\
f^{\mathrm{I}}_{r\theta,\mathrm{I}}(\theta) &= \tfrac{C_1\lambda_1}{\sqrt{2\pi}(\alpha-\beta)} \langle [-\lambda_1(\alpha-\beta)\cos(\lambda_1\pi/2) + (1+\beta)\sin(\lambda_1\pi)] \times \sin\{(\lambda_1+1)(\pi-\theta)\} \\
&\quad + [(\lambda_1-1)(\alpha-\beta)\sin(\lambda_1\pi/2)] \times \sin\{(\lambda_1-1)(\pi-\theta)\}\rangle \\
f^{\mathrm{II}}_{r\theta,\mathrm{I}}(\theta) &= \tfrac{C_2\lambda_2}{\sqrt{2\pi}(\alpha-\beta)} \langle [-\lambda_2(\alpha-\beta)\cos(\lambda_2\pi/2) - (1+\beta)\sin(\lambda_2\pi)] \times \cos\{(\lambda_2+1)(\pi-\theta)\} \\
&\quad + [(\lambda_2-1)(\alpha-\beta)\sin(\lambda_2\pi/2)] \times \cos\{(\lambda_2-1)(\pi-\theta)\}\rangle
\end{aligned}\right\} \tag{2b}$$

where

$$C_1 = \frac{(1-\beta)\sin\{3\lambda_1\pi/2\} - (1-\alpha)\sin\{\lambda_1\pi/2\} - \lambda_1(\alpha-\beta)}{(2+\beta+\alpha)\sin\{\lambda_1\pi/2\} - \lambda_1(\alpha-\beta)}$$
$$C_2 = \frac{(1-\beta)\sin\{3\lambda_2\pi/2\} - (1-\alpha)\sin\{\lambda_2\pi/2\} - \lambda_2(\alpha-\beta)}{(2+\beta+\alpha)\sin\{\lambda_2\pi/2\} - \lambda_2(\alpha-\beta)} \tag{2c}$$

Here, α, β, denote Dundurs bimaterial parameters α, β

$$\alpha = \frac{G_M(\kappa_I+1) - G_I(\kappa_M+1)}{G_M(\kappa_I+1) + G_I(\kappa_M+1)}, \quad \beta = \frac{G_M(\kappa_I-1) - G_I(\kappa_M-1)}{G_M(\kappa_I+1) + G_I(\kappa_M+1)}$$
$$\kappa_i = \begin{cases} (3-\nu_i)/(1+\nu_i) & \text{(plane stress)} \\ 3-4\nu_i & \text{(plane strain)} \end{cases} \quad (i = M, I) \tag{3}$$

Singular index λ_1, λ_2 around the corner A can be given from the following characteristic equations. Here, the singular indexes λ_1, λ_2 have real values in the range $0 < \mathrm{Re}(\lambda_i) < 1$ $(i = 1,2)$ when $\beta(\alpha-\beta) > 0$ (Chen and Nisitani, 1992)

$$\begin{aligned} D_1(\alpha,\beta,\gamma,\lambda) = {} & (\alpha-\beta)^2\lambda^2(1-\cos 2\gamma) + 2\lambda(\alpha-\beta)\sin\gamma\{\sin\lambda\gamma + \sin\lambda(2\pi-\gamma)\} \\ & + 2\lambda(\alpha-\beta)\beta\sin\gamma\{\sin\lambda(2\pi-\gamma) - \sin\lambda\gamma\} \\ & + (1-\alpha^2) - (1-\beta^2)\cos 2\lambda\pi + (\alpha^2-\beta^2)\cos\{2\lambda(\gamma-\pi)\} = 0 \\ D_2(\alpha,\beta,\gamma,\lambda) = {} & (\alpha-\beta)^2\lambda^2(1-\cos 2\gamma) - 2\lambda(\alpha-\beta)\sin\gamma\{\sin\lambda\gamma + \sin\lambda(2\pi-\gamma)\} \\ & - 2\lambda(\alpha-\beta)\beta\sin\gamma\{\sin\lambda(2\pi-\gamma) - \sin\lambda\gamma\} \\ & + (1-\alpha^2) - (1-\beta^2)\cos 2\lambda\pi + (\alpha^2-\beta^2)\cos\{2\lambda(\gamma-\pi)\} = 0 \end{aligned} \tag{4}$$

On the other hand, singular stress around the corner B can be expressed as follows:

$$\sigma_{ij,k} = \frac{K}{r^{1-\lambda}} f_{ij,k} \quad (ij = r,\ \theta,\ r\theta; k = M,\ I) \tag{5}$$

For matrix M $(0 \leqslant \theta \leqslant \pi/2)$,

$$\begin{aligned} f_{\theta,M}(\theta) &= m_1\cos\{(\lambda-1)\theta\} - m_2\sin\{(\lambda-1)\theta\} - m_1\cos\{(\lambda+1)\theta\} + m_3\sin\{(\lambda+1)\theta\} \\ f_{r\theta,M}(\theta) &= m_3\cos\{(\lambda-1)\theta\} + m_4\sin\{(\lambda-1)\theta\} - m_3\cos\{(\lambda+1)\theta\} - m_1\sin\{(\lambda+1)\theta\} \\ m_1 &= \lambda(\lambda+1)Y_2, \quad m_2 = \lambda(\lambda+1)Y_1, \quad m_3 = \lambda(\lambda-1)Y_1, \quad m_4 = \lambda(\lambda-1)Y_2 \end{aligned} \tag{6a}$$

For inclusion I $(\pi/2 \leqslant \theta \leqslant \pi)$

$$\begin{aligned} f_{\theta,I}(\theta) &= M_1\cos\{(\lambda-1)(\pi-\theta)\} - M_2\sin\{(\lambda-1)(\pi-\theta)\} - M_1\cos\{(\lambda+1)(\pi-\theta)\} + M_3\sin\{(\lambda+1)(\pi-\theta)\} \\ f_{r\theta,I}(\theta) &= -M_3\cos\{(\lambda-1)(\pi-\theta)\} - M_4\sin\{(\lambda-1)(\pi-\theta)\} + M_3\cos\{(\lambda+1)(\pi-\theta)\} + M_1\sin\{(\lambda+1)(\pi-\theta)\} \\ M_1 &= \lambda(\lambda+1)L_2Y_4/L_1,\ \ M_2 = \lambda(\lambda+1)L_2Y_3/L_1,\ \ M_3 = \lambda(\lambda-1)L_2Y_3/L_1,\ \ M_4 = \lambda(\lambda-1)L_2Y_4/L_1 \end{aligned} \tag{6b}$$

where

$$\begin{aligned} & Y_1 = 4\lambda\beta\cos(\lambda\pi) + 2\beta[\cos(\lambda\pi) - 1] + 4\lambda(\lambda+1)(\alpha-\beta), \quad Y_2 = 2(2\lambda\beta-1)\sin(\lambda\pi), \quad Y_3 = -Y_1, \\ & Y_4 = -2(2\lambda\beta+1)\sin(\lambda\pi), \quad L_1 = 2\lambda\cos(\lambda\pi/2)Y_4 - 2(\lambda-1)\sin(\lambda\pi/2)Y_3, \\ & L_2 = -2\lambda\cos(\lambda\pi/2)Y_2 + 2(\lambda-1)\sin(\lambda\pi/2)Y_1 \end{aligned} \tag{6c}$$

Singular index λ around the corner B can be given from the following characteristic equation. Here, the singular index has a real value in the range $0 < \mathrm{Re}(\lambda) < 1$ when $\alpha(\alpha - 2\beta) > 0$ (Chen and Nisitani, 1993).

Table 1
Singular index λ_1, λ_2 the corner A and singular index λ at the corner B for Fig. 1 under plane strain with $\nu_M = \nu_I = 0.3$

	Corner A		Corner B
	λ_1	λ_2	λ
$G_I/G_M = 2$	0.9109102	0.9788427	0.9630015
$G_I/G_M = 10$	0.7981112	0.7856547	0.8015335
$G_I/G_M = 60$	0.7659920	0.6383511	0.7289061
$G_I/G_M = 100$	0.7632349	0.6218440	0.7219664
$G_I/G_M \to \infty$	0.7590420	0.5951564	0.7111729

$$D(\alpha,\beta,\gamma,\lambda)|_{\gamma=\pi/2} = [\cos^2(\lambda\pi/2) - (1-\lambda)^2]^2\beta^2 + 2(1-\lambda)^2[\cos^2(\lambda\pi/2) - (1-\lambda)^2]\alpha\beta + (1-\lambda)^2[(1-\lambda)^2 - 1]\alpha^2 + \cos^2(\lambda\pi/2)\sin^2(\lambda\pi/2) = 0 \tag{7}$$

Table 1 indicates several examples of λ_1, λ_2 for corner A, and λ for corner B, which is obtained from Eqs. (4) and (7).

3. Method of analysis

The present method of analysis is essentially based on the body force method coupled with singular integral equation formulation, which yields accurate numerical solutions. The detail may be found in (Noda et al., 1996; Noda and Matsuo, 1998).

3.1. Singular integral equations of the body force method

There have been little discussions regarding the singular stress at the fiber end B. In this study, therefore, first we consider tension problems as shown in Fig. 2(a) and (b) and compare the results each other. The method of analysis will be explained for Fig. 2(a). The solution for Fig. 1 can be expressed similarly except for the stress at infinity σ_x^∞. Here, l_x and l_y are dimensions of inclusions, and denote the shear modulus and Poisson's ratio of the matrix by G_M and ν_M and the inclusion by G_I and ν_I. The body force method requires fundamental solutions, that is, the stress and displacement fields in a semi-infinite body due to a point force, $h_{nn}^{F_{nM}}$, etc (Nisitani, 1967). Similar expressions due to a ring force in a semi-infinite body for Fig. 1(b) are found in (Noda and Moriyama, 2004). Then, the problem can be expressed as a system of singular integral Eqs. (5) and (6) , where the unknowns are body forces densities F_{nM}, F_{tM}, F_{nI}, F_{tI} distributed in the normal and tangential directions along the fictitious boundary in two semi-infinite plates, 'M' and 'I'. Here, the

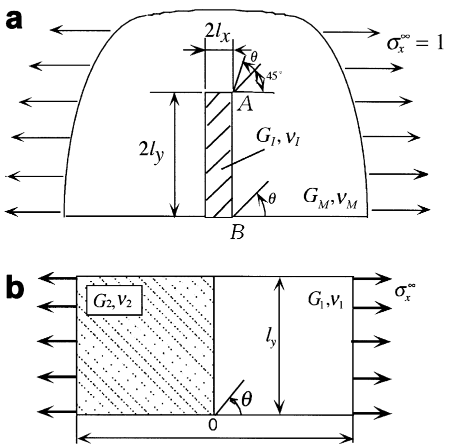

Fig. 2. (a) A rectangular inclusion model in a semi-infinite plate under tension (b) A bonded strip under tension.

semi-infinite plate '*M*' has the same elastic constants as those of the matrix, and the semi-infinite plate '*I*' has the same elastic constants as those of the inclusion.

$$\left.\begin{aligned}
&-\tfrac{1}{2}F_{nM}(s)-\tfrac{1}{2}F_{nI}(s)+\int_L h_{nn}^{F_{nM}}(r,s)F_{nM}(r)\mathrm{d}r+\int_L h_{nn}^{F_{tM}}(r,s)F_{tM}(r)\mathrm{d}r-\int_L h_{nn}^{F_{nI}}(r,s)F_{nI}(r)\mathrm{d}r\\
&-\int_L h_{nn}^{F_{tI}}(r,s)F_{tI}(r)\mathrm{d}r=-\sigma_{nM}^{\infty}(s)+\sigma_{nI}^{\infty}(s)-\tfrac{1}{2}F_{tM}(s)-\tfrac{1}{2}F_{tI}(s)+\int_L h_{nt}^{F_{nM}}(r,s)F_{nM}(r)\mathrm{d}r\\
&+\int_L h_{nt}^{F_{tM}}(r,s)F_{tM}(r)\mathrm{d}r-\int_L h_{nt}^{F_{nI}}(r,s)F_{nI}(r)\mathrm{d}r-\int_L h_{nt}^{F_{tI}}(r,s)F_{tI}(r)\mathrm{d}r=-\tau_{ntM}^{\infty}(s)+\tau_{ntI}^{\infty}(s)
\end{aligned}\right\}\tag{8}$$

$$\left.\begin{aligned}
&\int_L h_{u}^{F_{nM}}(r,s)F_{nM}(r)\mathrm{d}r+\int_L h_{u}^{F_{tM}}(r,s)F_{tM}(r)\mathrm{d}r-\int_L h_{u}^{F_{nI}}(r,s)F_{nI}(r)\mathrm{d}r-\int_L h_{u}^{F_{tI}}(r,s)F_{tI}(r)\mathrm{d}r=-u_M^{\infty}+u_I^{\infty}\\
&\int_L h_{v}^{F_{nM}}(r,s)F_{nM}(r)\mathrm{d}r+\int_L h_{v}^{F_{tM}}(r,s)F_{tM}(r)\mathrm{d}r-\int_L h_{v}^{F_{nI}}(r,s)F_{nI}(r)\mathrm{d}r-\int_L h_{v}^{F_{tI}}(r,s)F_{tI}(r)\mathrm{d}r=-v_M^{\infty}+v_I^{\infty}
\end{aligned}\right\}\tag{9}$$

Eqs. (8) and (9) mean the boundary conditions $\sigma_{nM}=\sigma_{nI}$, $\tau_{ntM}=\tau_{ntI}$, $u_M=u_I$, $v_M=v_I$. Here, the notation σ_{nM}^{∞} is a remote tensile stress at infinity.

3.2. Numerical solutions around corner A

Fig. 3 illustrates boundary divisions for numerical solution of Eqs. (8) and (9). First, the method of analysis will be explained by taking an example for corner A. Around corner A, the body forces acting in the normal and tangential directions, F_n and F_t, should be expressed as two types, that is, symmetric mode I type $r_1^{\lambda_1-1}$ and skew-symmetric mode II type $r_1^{\lambda_2-1}$ to the bisector of the corners. The body force densities distributed around

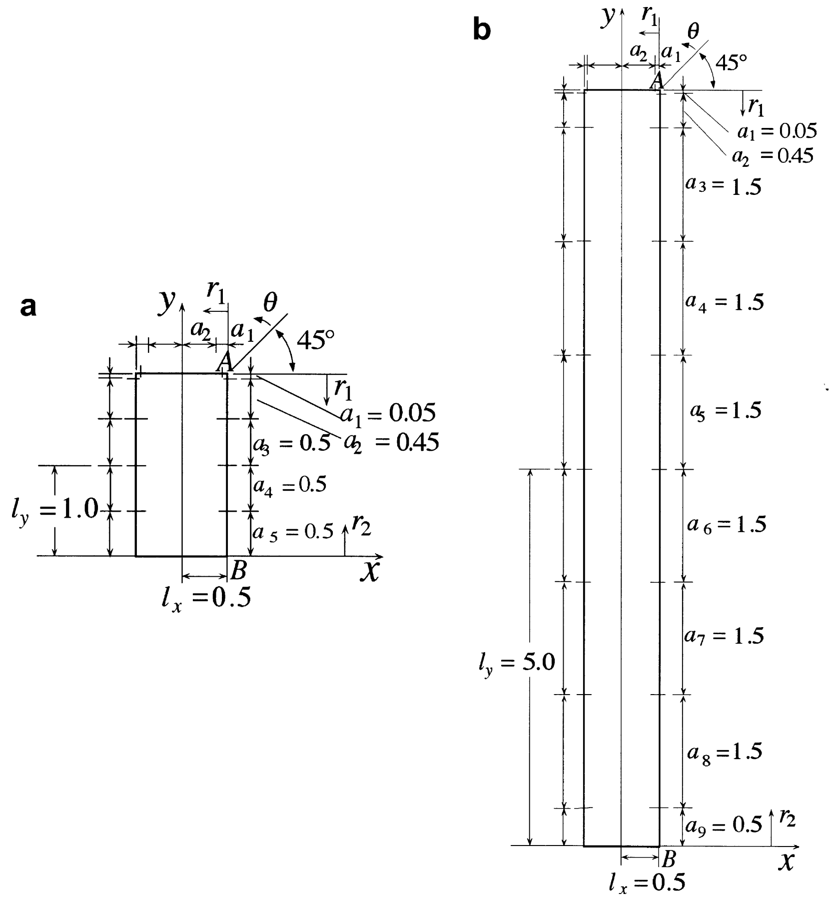

Fig. 3. Boundary division ((a) $l_y/l_x = 2$, (b) $l_y/l_x = 10$).

corner A may be expressed as Eqs. (10) and (11) using fundamental densities $r_1^{\lambda_1-1}$, $r_1^{\lambda_2-1}$ and weight functions W_{nM}^{I}–W_{tM}^{II} (Chen and Nisitani, 1992).

$$\left.\begin{aligned} F_{nM}(r_1) &= F_{nM}^{\mathrm{I}}(r_1) + F_{nM}^{\mathrm{II}}(r_1) = W_{nM}^{\mathrm{I}}(r_1)r_1^{\lambda_1-1} + W_{nM}^{\mathrm{II}}(r_1)r_1^{\lambda_2-1} \\ F_{tM}(r_1) &= F_{tM}^{\mathrm{I}}(r_1) + F_{tM}^{\mathrm{II}}(r_1) = W_{tM}^{\mathrm{I}}(r_1)r_1^{\lambda_1-1} + W_{tM}^{\mathrm{II}}(r_1)r_1^{\lambda_2-1} \\ F_{nI}(r_1) &= F_{nI}^{\mathrm{I}}(r_1) + F_{nI}^{\mathrm{II}}(r_1) = W_{nI}^{\mathrm{I}}(r_1)r_1^{\lambda_1-1} + W_{nI}^{\mathrm{II}}(r_1)r_1^{\lambda_2-1} \\ F_{tI}(r_1) &= F_{tI}^{\mathrm{I}}(r_1) + F_{tI}^{\mathrm{II}}(r_1) = W_{tI}^{\mathrm{I}}(r_1)r_1^{\lambda_1-1} + W_{tI}^{\mathrm{II}}(r_1)r_1^{\lambda_2-1} \end{aligned}\right\} \tag{10}$$

$$\left.\begin{aligned} W_{nM}^{\mathrm{I}}(r_1) &= \sum_{n=1}^{M} a_n r_1^{n-1}, \quad W_{tM}^{\mathrm{I}}(r_1) = \sum_{n=1}^{M} b_n r_1^{n-1} \\ W_{nM}^{\mathrm{II}}(r_1) &= \sum_{n=1}^{M} c_n r_1^{n-1}, \quad W_{tM}^{\mathrm{II}}(r_1) = \sum_{n=1}^{M} d_n r_1^{n-1} \\ W_{nI}^{\mathrm{I}}(r_1) &= \sum_{n=1}^{M} e_n r_1^{n-1}, \quad W_{tI}^{\mathrm{I}}(r_1) = \sum_{n=1}^{M} f_n r_1^{n-1} \\ W_{nI}^{\mathrm{II}}(r_1) &= \sum_{n=1}^{M} g_n r_1^{n-1}, \quad W_{tI}^{\mathrm{II}}(r_1) = \sum_{n=1}^{M} h_n r_1^{n-1} \end{aligned}\right\} \tag{11}$$

Eqs. (10) and (11) do not include the terms expressing local uniform stretching and shear distortion at the corner A. Therefore the stress σ_n^∞ applied in the plate 'I' is used to express local uniform stretching and shear distortion at the corner A. On the numerical solution as shown in Eqs. (10) and (11), the singular integral Eqs. (8) and (9) are reduced to algebraic equations for the determination of the unknown coefficients a_n–h_n. These coefficients are determined from the boundary conditions at suitably chosen collocation points. It should be noted that the body force densities are difficult to be obtained directly because they tend to go infinity at the corner A. However, the weight functions W_{nM}^{I}, W_{tM}^{I}, etc. may be obtained accurately because they have finite values at the corner A. The generalized stress intensity factors K_{I,λ_1}, $K_{\mathrm{II},\lambda_2}$ for angular corners can be obtained from the values of $W_n^{\mathrm{I}}(0)$, $W_n^{\mathrm{II}}(0)$, $W_t^{\mathrm{I}}(0)$, $W_t^{\mathrm{II}}(0)$ at the corner tip (Noda et al., 1998).

3.3. Numerical solutions around the corner B

Excluding around the corner A, symmetric and skew-symmetric types of distributions of body forces are not applied. For example, Eq. (12) can be applied for corner B.

$$\left.\begin{aligned} F_{nM}(r_2) &= W_{nM}(r_2)r_2^{\lambda-1}, \quad W_{nM}(r_2) = \sum_{n=1}^{M} i_n r_2^{n-1} \\ F_{tM}(r_2) &= W_{tM}(r_2)r_2^{\lambda-1}, \quad W_{tM}(r_2) = \sum_{n=1}^{M} j_n r_2^{n-1} \\ F_{nI}(r_2) &= W_{nI}(r_2)r_2^{\lambda-1}, \quad W_{nI}(r_2) = \sum_{n=1}^{M} k_n r_2^{n-1} \\ F_{tI}(r_2) &= W_{tI}(r_2)r_2^{\lambda-1}, \quad W_{tI}(r_2) = \sum_{n=1}^{M} l_n r_2^{n-1} \end{aligned}\right\} \tag{12}$$

The generalized stress intensity factors K can be obtained from the values of $W_n^{\mathrm{I}}(0)$, $W_n^{\mathrm{II}}(0)$, $W_t^{\mathrm{I}}(0)$, $W_t^{\mathrm{II}}(0)$ at corner B (Noda et al., 1998).

Consider force distributions in the θ- and r-directions whose magnitudes are proportional to $P \times r^{\lambda-1}$ and $Q \times r^{\lambda-1}$ in a semi-infinite plate (see Fig. 4). The stresses due to those force distributions are given from the following stress functions.

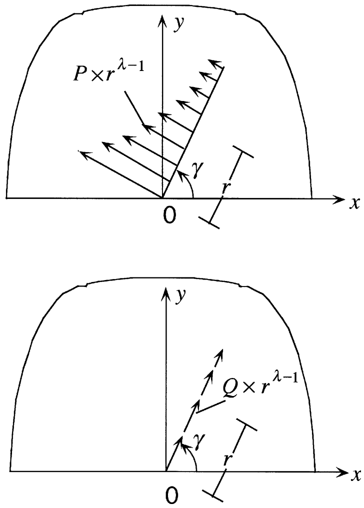

Fig. 4. Distribution of the body force, which are proportional to $r^{\lambda-1}$.

$$\left.\begin{aligned}
&\sigma_{\theta j}+\sigma_{rj}=\mathrm{Re}[4\phi'_{j(z)}]\\
&\sigma_{\theta j}-\sigma_{rj}+2i\tau_{r\theta j}=2\mathrm{e}^{2i\theta}\{\bar{z}\phi''_{j(z)}+\varphi'_{j(z)}\}
\end{aligned}\right\}\quad (j=1,2) \tag{13}$$

where

$$\left.\begin{aligned}
&\left.\begin{aligned}\phi_{j(z)}&=a_j z^\lambda\\ \varphi_{j(z)}&=b_j z^\lambda\end{aligned}\right\}\\
&a_1=\frac{X(\mathrm{e}^{2\mathrm{i}\lambda\pi}+\kappa\mathrm{e}^{2\mathrm{i}\lambda\gamma})-\lambda\overline{X}(\mathrm{e}^{2\mathrm{i}\gamma}-1)}{\mathrm{e}^{2\mathrm{i}\lambda\pi}-1}\\
&a_2=\frac{X(1+\kappa\mathrm{e}^{2\mathrm{i}\lambda\pi})-\lambda\overline{X}(\mathrm{e}^{2\mathrm{i}\gamma}-1)}{\mathrm{e}^{2\mathrm{i}\lambda\pi}-1}\\
&b_1=-\lambda a_1-\bar{a}_1\\
&b_2=-\lambda a_2-\mathrm{e}^{-2\mathrm{i}\lambda\pi}a_2\\
&\kappa=\begin{cases}(3-v)/(1+v)\\ 3-4v\end{cases}\\
&X=\frac{(P-\mathrm{i}Q)\mathrm{e}^{-\mathrm{i}(\lambda-1)\gamma}}{\lambda(\kappa+1)}
\end{aligned}\right\} \tag{14}$$

By substitute $\theta=\pi/2$ into θ in Eq. (13), we have

$$\left.\begin{aligned}
&\sigma_{xj}=2\mathrm{Re}[\phi'_{j(z)}]-\mathrm{Re}[\bar{z}\phi''_{j(z)}+\varphi'_{j(z)}]=s_{\sigma j}\times r^{\lambda-1}\\
&\tau_{xyj}=-\mathrm{Im}[\bar{z}\phi''_{j(z)}+\varphi'_{j(z)}]=s_{\tau j}\times r^{\lambda-1}\\
&s_{\sigma j}=2\{\mathrm{Re}[a_j]\lambda\cos(\gamma(\lambda-1))-\mathrm{Im}[a_j]\lambda\sin(\gamma(\lambda-1))\}\\
&\qquad+\{-\mathrm{Re}[a_j]\lambda(\lambda-1)\cos(\gamma(\lambda-3))+\mathrm{Im}[a_j]\lambda(\lambda-1)\sin(\gamma(\lambda-3))\}\\
&\qquad+\{\mathrm{Re}[b_j]\lambda\cos(\gamma(\lambda-1))-\mathrm{Im}[b_j]\lambda\sin(\gamma(\lambda-1))\}\\
&s_{\tau j}=\{\mathrm{Re}[a_j]\lambda(\lambda-1)\sin(\gamma(\lambda-3))+\mathrm{Im}[a_j]\lambda(\lambda-1)\cos(\gamma(\lambda-3))\}\\
&\qquad-\{\mathrm{Re}[b_j]\lambda\sin(\gamma(\lambda-1))+\mathrm{Im}[b_j]\lambda\cos(\gamma(\lambda-1))\}
\end{aligned}\right\} \tag{15}$$

From Eqs. (5) and (15), we can see $K=\sigma_{xj}r^{1-\lambda}/f_{\theta\theta}=s_{\sigma j}/f_{\theta\theta}$, and $K=\tau_{xyj}r^{1-\lambda}/f_{r\theta}=s_{\tau j}/f_{r\theta}$. By putting $P=W_{nM}(0)$, $Q=W_{tM}(0)$, $v=v_M$ (or $P=W_{nI}(0)$, $Q=W_{tI}(0)$, $v=v_I$), $\gamma=\pi/2$ in Eq. (14), generalized stress intensity factor K will be obtained.

4. Numerical results and discussion

In the following discussion, the stress intensity factors $F_{\sigma,\mathrm{I}}$, $F_{\sigma,\mathrm{II}}$ defined as (16) will be used to express the intensity of singular stress at the corner A. On the other hand, the stress intensity factor F_σ defined as (17) will be used to express the one at corner B.

Table 2
Convergence of $F_{\sigma,\mathrm{I}}(A)$, $F_{\sigma,\mathrm{II}}(A)$ and $F_\sigma(B)$ when $l_y/l_x=2$, $G_I/G_M=10$ (M: number of collocation points) (a) in Fig. 2(a), (b) in Fig. 1(a), (c) in Fig. 1(b)

M	$F_{\sigma,\mathrm{I}}(A)$	$F_{\sigma,\mathrm{II}}(A)$	$F_\sigma(B)$	
(a)				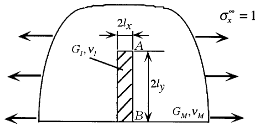
4	0.158	0.613	0.226	
5	0.157	0.612	0.217	
6	0.157	0.617	0.216	
(b)				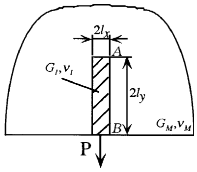
4	0.0283	0.0362	0.199	
5	0.0284	0.0363	0.191	
6	0.0284	0.0364	0.191	
(c)				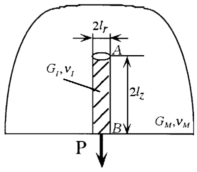
4	0.499	0.923	1.460	
5	0.489	0.937	1.473	
6	0.482	0.948	1.473	

Table 3
F_σ at the corner O for bonded strip in Fig. 5

α	β						
	−0.2	−0.1	0.0	0.1	0.2	0.3	0.4
0.05	0.862 (0.87)	0.924 (0.93)	–	–	–	–	–
0.1	0.767 (0.79)	0.890 (0.89)	0.955 (0.96)	–			
0.15	0.698 (0.71)	–	–	–			
0.2	–	0.797 (0.81)	0.889 (0.90)	–	–	–	–
0.3	–	0.697 (0.71)	0.796 (0.81)	0.913 (0.93)	–	–	–
0.4	–	0.615 (0.62)	0.718 (0.72)	0.822 (0.83)	–	–	–
0.5	–	–	0.635 (0.64)	0.722 (0.73)	0.842 (0.87)	–	–
0.6	–	–	0.559 (0.56)	0.638 (0.64)	0.724 (0.74)	–	–
0.7	–	–	0.486 (0.49)	0.558 (0.56)	0.626 (0.64)	0.800 (0.81)	–
0.75	–	–	–	–	–	0.712 (0.73)	–
0.8	–	–	0.450 (0.45)	0.487 (0.49)	0.538 (0.55)	0.636 (0.65)	–
0.85	–	–	–	–	–	0.582 (0.60)	0.835 (0.83)
0.9	–	–	0.381 (0.39)	0.412 (0-42)	0.456 (0.46)	0.534 (0.55)	0.726 (0.72)
0.95	–	–	–	–	–	–	0.643 (0.64)
1.0	–	–	0.332 (0.33)	0.357 (0.35)	0.395 (0.40)	0.446 (0.44)	0.540 (0.54)

Present Analysis
( ):Chen and Nisitani(1993)

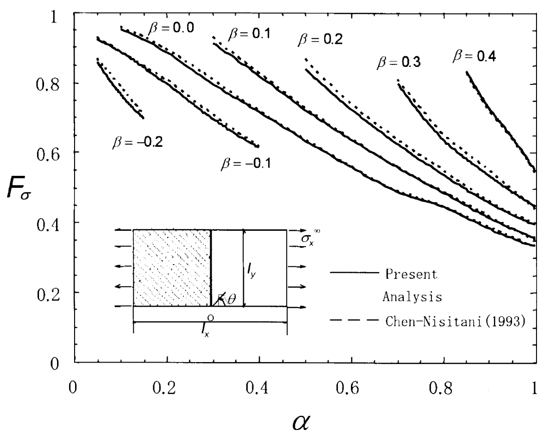

Fig. 5. F_σ at the corner O for tension $\sigma_\theta|_{\theta=90^\circ} = \frac{F_\sigma}{(r/l_y)^{1-\lambda}}$.

Table 4
Stress intensity factor F_σ in Fig. 2 (a) at the corner A and B (plane strain, $\nu_M = \nu_I = 0.3$)

l_y/l_x	G_I/G_M											
	$F_{\sigma,\mathrm{I}}(A)$				$F_{\sigma,\mathrm{II}}(A)$				$F_\sigma(B)$			
	2	10	60	100	2	10	60	100	2	10	60	100
2	0.235	0.158	0.120	0.116	0.629	0.613	0.493	0.479	0.803	0.219	0.110	0.102
5	0.230	0.175	0.152	0.150	0.635	0.601	0.473	0.459	0.795	0.203	0.101	0.093
10	0.229	0.182	0.164	0.163	0.636	0.593	0.464	0.450	0.785	0.183	0.088	0.081
30	0.229	0.188	0.173	0.172	0.636	0.588	0.457	0.443	0.759	0.151	0.066	0.060

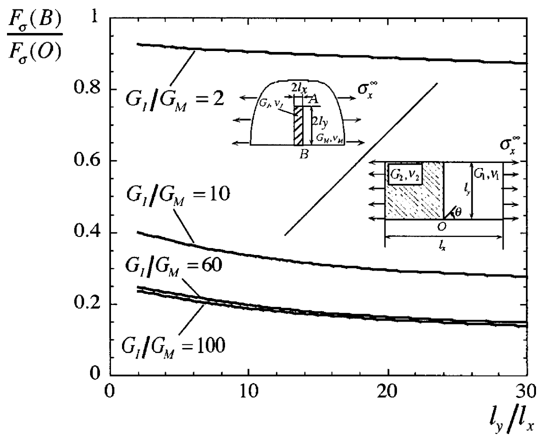

Fig. 6. Ratio of F_σ at B to F_σ at O (plane strain, $\nu_M = \nu_I = 0.3$).

For corner A in Figs. 1 and 2

$$
\left.
\begin{aligned}
\sigma_{\theta M}|_{\theta=\pm 135^\circ} = \sigma_{\theta I}|_{\theta=\pm 135^\circ} &= \frac{K_{\mathrm{I},\lambda_1}}{r^{1-\lambda_1}} f_\theta^{\mathrm{I}}\Big|_{\theta=\pm 135^\circ} \mp \frac{K_{\mathrm{II},\lambda_2}}{r^{1-\lambda_2}} f_\theta^{\mathrm{II}}\Big|_{\theta=\pm 135^\circ} \\
&= \frac{\sigma F_{\sigma,\mathrm{I}}}{(r/l_x)^{1-\lambda_1}} \mp \frac{\sigma F_{\sigma,\mathrm{II}}}{(r/l_x)^{1-\lambda_2}}
\end{aligned}
\right\} \tag{16}
$$

For corner B in Figs. 1 and 2 (For corner O in Fig. 2(b))

Table 5
$F_\sigma(B)$ for a rectangular inclusion when $l_y/l_x = 10$ under double pullout forces (plane strain, $\nu_M = \nu_I = 0.3$, l = spacing of double force(see Fig. 7))

l/l_x	G_I/G_M		
	$F_\sigma(B)$		
	10	60	100
0	0.202	0.176	0.173
1/4	0.217	0.190	0.187
1/3	0.230	0.203	0.200
1/2	0.273	0.246	0.243
2/3	0.356	0.338	0.335

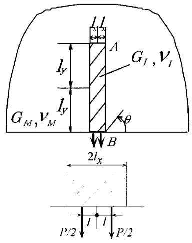

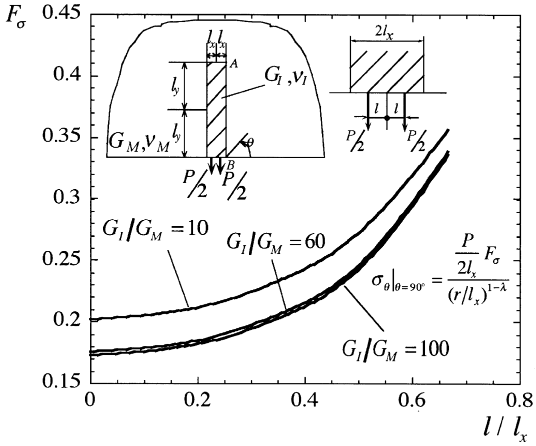

Fig. 7. Stress intensity factor $F_\sigma(B)$ for a rectangular inclusion under double pull out forces when $l_y/l_x = 10$ (plane strain, $\nu_M = \nu_I = 0.3$).

Table 6
$F_{\sigma,\mathrm{I}}(A)$, $F_{\sigma,\mathrm{II}}(A)$, and $F_\sigma(B)$ for a rectangular inclusion (a) under a single pullout force (b) under double pullout force (plane strain, $\nu_M = \nu_I = 0.3$)

l_y/l_x	G_I/G_M								
	$F_{\sigma,\mathrm{I}}(A)$			$F_{\sigma,\mathrm{II}}(A)$			$F_\sigma(B)$		
	10	60	100	10	60	100	10	60	100
(a)									
2	0.0284	0.0182	0.0171	0.0363	0.0202	0.0189	0.191	0.170	0.168
4	0.0027	0.0018	0.0022	0.0050	0.0007	0.0011	0.202	0.176	0.173
8	0.0015	0.0002	0.0004	0.0024	0.0007	0.0002	0.202	0.176	0.173
10	0.0013	0.0001	0.0002	0.0019	0.0005	0.0001	0.202	0.176	0.173
20	0.0006	0.0001	0.0002	0.0009	0.0002	0.0002	0.204	0.178	0.175
30	0.0003	0.0001	0.0001	0.0005	0.0001	0.0002	0.205	0.178	0.175
(b)									
2	0.0227	0.0120	0.0108	0.0291	0.0139	0.0127	0.263	0.242	0.239
4	0.0029	0.0015	0.0019	0.0050	0.0006	0.0010	0.272	0.246	0.243
8	0.0015	0.0002	0.0004	0.0024	0.0001	0.0002	0.272	0.246	0.243
10	0.0013	0.0001	0.0002	0.0019	0.0001	0.0001	0.273	0.246	0.243
20	0.0006	0.0001	0.0002	0.0010	0.0001	0.0001	0.273	0.246	0.243
30	0.0003	0.0001	0.0002	0.0005	0.0002	0.0002	0.273	0.246	0.243

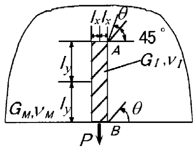

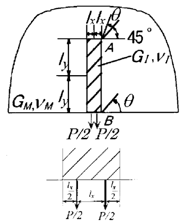

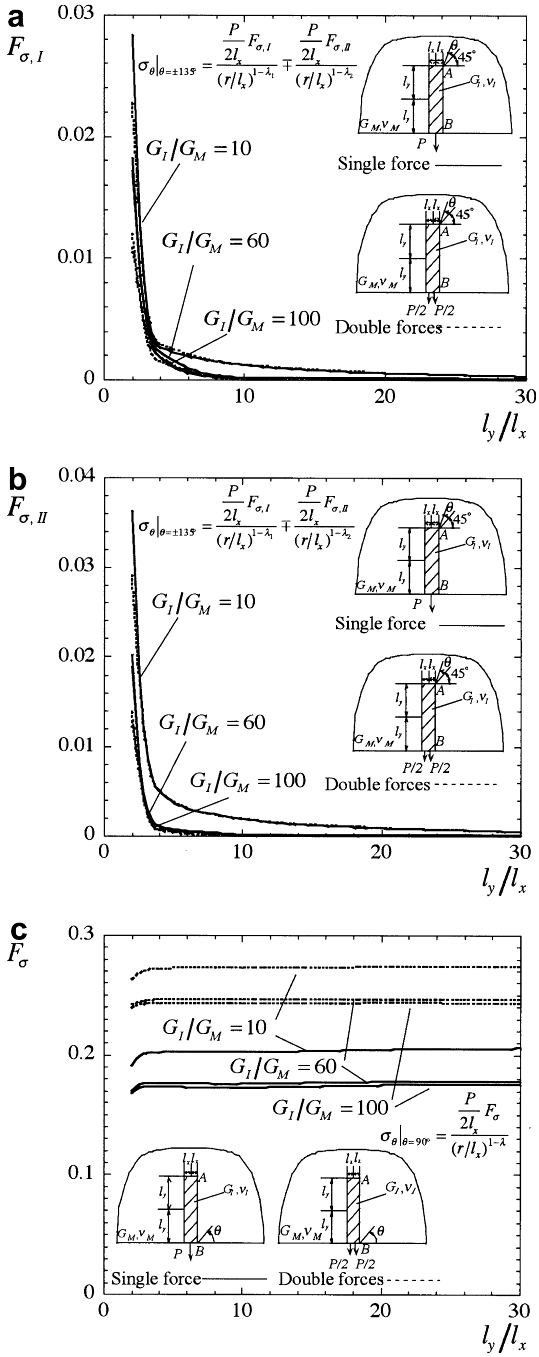

Fig. 8. Stress intensity factors (a) $F_{\sigma,\mathrm{I}}(A)$, (b) $F_{\sigma,\mathrm{II}}(A)$, and (c) $F_\sigma(B)$ for a rectangular inclusion under pull out force $l_y/l_x = 10$ (plane strain, $v_M = v_I = 0.3$).

$$\sigma_{\theta M}|_{\theta=90^\circ} = \sigma_{\theta I}|_{\theta=90^\circ} = \frac{K}{r^{1-\lambda}}f_\theta = \frac{\sigma F_\sigma}{(r/l_x)^{1-\lambda}} \tag{17}$$

Here, we put $\sigma = P/(2l_x)$ (for Fig. 1(a)), $\sigma = P/(\pi l_r^2)$ (for Fig. 1(b)), $\sigma = \sigma_x^\infty$ (for Fig. 2(a)).

Table 7
$F_{\sigma,\mathrm{I}}(A)$, $F_{\sigma,\mathrm{II}}(A)$, and $F_{\sigma}(B)$ for a cylindrical inclusion under pullout force

l_z/l_r	G_I/G_M								
	$F_{\sigma,\mathrm{I}}(A)$			$F_{\sigma,\mathrm{II}}(A)$			$F_{\sigma}(B)$		
	10	60	100	10	60	100	10	60	100
2	0.486	3.109	5.210	0.943	4.601	7.414	1.473	7.736	12.65
4	0.220	1.851	3.191	0.452	2.802	4.634	1.222	5.129	8.084
8	0.070	0.943	1.737	0.151	1.449	2.551	1.154	3.774	5.509
10	0.044	0.723	1.379	0.098	1.115	2.031	1.154	3.558	5.042
20	0.009	0.246	0.554	0.021	0.384	0.823	1.182	3.295	4.325
30	0.003	0.101	0.257	0.008	0.159	0.384	1.183	3.207	4.112

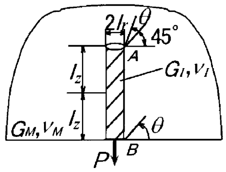

4.1. Convergence of the results

Table 2 indicates examples of stress intensity factors $F_{\sigma,\mathrm{I}}(A)$, $F_{\sigma,\mathrm{II}}(A)$, $F_{\sigma}(B)$ for the problems of Figs. 1 and 2 (a). Here, the boundary division as shown in Fig. 3 is applied. Table 2 shows good convergence to the third digit. Similar results can be seen for other cases. Then, it is confirmed that the values of $F_{\sigma,\mathrm{I}}(A)$, $F_{\sigma,\mathrm{II}}(A)$, $F_{\sigma}(B)$ have convergence to the third digit in most cases when the number of collocation points $M = 4$–6.

4.2. Stress intensity factors of a bonded strip and a fiber in a semi-infinite plate under tension

Little results are available for reliable generalized stress intensity factors regarding the edge point B in Fig. 1. Therefore, first, we analyzed tension problems forFig. 2(a) and (b) to compare the results each other. Here, a similar method is applied to the bonded strip for Fig. 2(b), whose elastic constants are G_1, ν_1 and G_2, ν_2. Table 3 and Fig. 5 indicate the results of F_{σ} at the edge point O in Fig. 2(b) when $l_x/l_y = 2$ and Dundurs parameter $\beta = -0.2, -0.1, 0, \ldots, 0.4$. The previous results given from the figure in (Chen and Nisitani, 1992) coincide with the present results within 3% error.

Table 4 shows the results for a fiber under transverse tension when $l_y/l_x = 2$, 5, 10. Fig. 6 shows $F_{\sigma}(B)/F_{\sigma}(O)$ where $F_{\sigma}(B)$ is the result at corner B in Fig. 2 (a), and $F_{\sigma}(O)$ is the result in Fig. 2 (b). The value of $F_{\sigma}(B)/F_{\sigma}(O)$ decreases with increasing l_y/l_x, and becomes constant as $l_y/l_x \to \infty$. For large value of G_I/G_M, the value becomes smaller. The value of $F_{\sigma}(B)/F_{\sigma}(O)$ is mainly controlled by G_I/G_M and insensitive to l_y/l_x.

4.3. Stress intensity factors of a fiber under pullout force

For carbon fiber-reinforced composites, the elastic modulus ratio is usually in the range of $G_I/G_M = 61$–118, and for glass fiber-reinforced composites, $G_I/G_M = 24$–84 (Noda and Takase, 2005). In this analysis, we put $G_I/G_M = 10$, 60, 100. Table 5 and Fig. 7 show the results of $F_{\sigma}(B)$ at the corner B with varying the position of pullout forces. The value of F_{σ} increases as the force approaches the corner B. In the range of $0 \leqslant l/l_x \leqslant 2/3$, F_{σ} becomes larger by 1.9 times.

Table 6 shows the results of single pullout force when $l = 0$ and the results of double pullout forces when $l = l_x/2$. Here, the aspect ratio of the rectangular inclusion is assumed as $l_y/l_x = 2$, 4, 8, 10, 20, 30. The values of $F_{\sigma,\mathrm{I}}(A)$, $F_{\sigma,\mathrm{II}}(A)$, $F_{\sigma}(B)$ are plotted in Fig. 8. At the corner A, the results for single and double forces have almost no difference. At the corner B, the difference for single and double forces is 30-40 percent. From Fig. 8, it us found that if the aspect ratio of the fiber $l_y/l_x \geqslant 4$ the results are almost constant. In other words, the effective length is $l_y/l_x = 4$ for large aspect ratio of the fiber.

Table 7 and Fig. 9(a)–(c) shows the results of cylindrical inclusion under single pullout force. From Figs. 8 and 9, it is seen that the values of $F_{\sigma,\mathrm{I}}$, $F_{\sigma,\mathrm{II}}$ approach zero with increasing the aspect ratio l_y/l_x. On the other

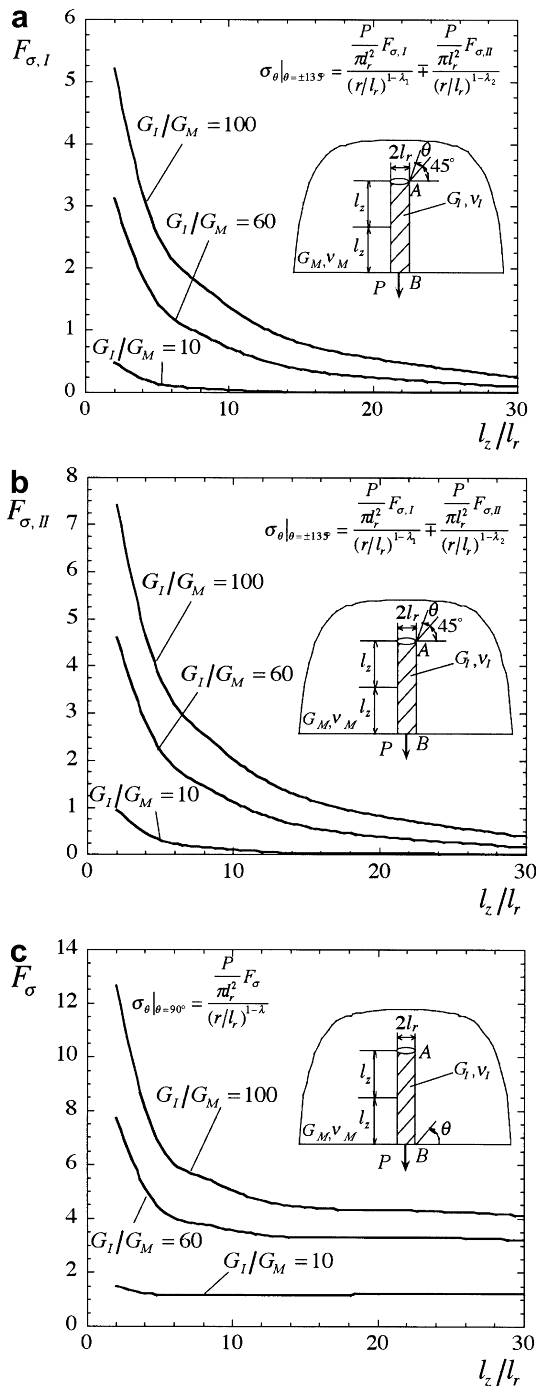

Fig. 9. Stress intensity factors (a) $F_{\sigma,\mathrm{I}}(A)$, (b) $F_{\sigma,\mathrm{II}}(A)$, and (c) $F_\sigma(B)$ for a cylindrical inclusion under pull-out force.

hand, the value of F_σ for rectangular and cylindrical inclusions becomes constant at $l_y/l_x \cong 10$ for each value of G_I/G_M. From Fig. 9, it may be concluded that the effective fiber length is $l_z/l_r = 30$ for large aspect ratio $l_z/l_r \geqslant 30$.

5. Conclusion

Fiber pullout problems have been investigated in many years. However, there are few studies treating the singular stress at the fiber ends, which may cause fiber debonding. In this paper, the intensities of singular stresses at the interfacial ends were analyzed and discussed with varying

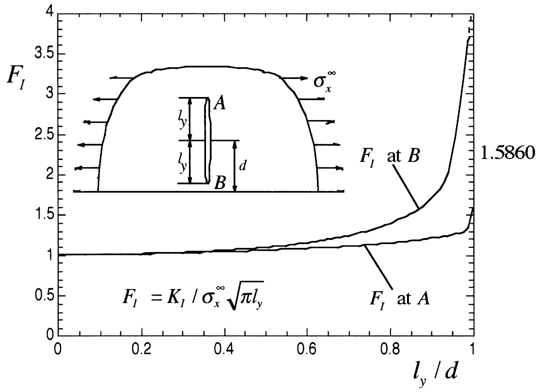

Fig. A1. Stress intensity factors F_I at A and B for an internal crack in a half-plane.

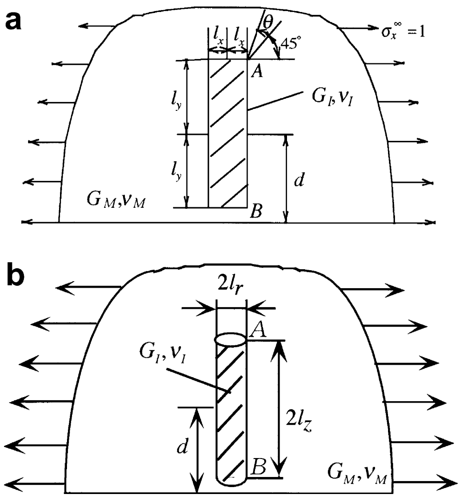

Fig. A2. (a) A rectangular inclusion in a semi-infinite plate under tension (b) A cylindrical inclusion in a semi-infinite body under biaxial tension.

Table A1
$F_{\sigma,\text{I}}$ and $F_{\sigma,\text{II}}$ at the corner A and B for a rectangular inclusion when $l_y/l_x = 10$ (plane strain, $v_M = v_I = 0.3$)

G_I/G_M	$F_{\sigma,\text{I}}$ at A			$F_{\sigma,\text{II}}$ at A			$F_{\sigma,\text{I}}$ at B			$F_{\sigma,\text{II}}$ at B		
l_y/d	2	10	100	2	10	100	2	10	100	2	10	100
→0.0	0.228	0.126	0.057	0.658	0.670	0.557	0.228	0.126	0.057	0.658	0.670	0.557
0.1	0.228	0.127	0.058	0.656	0.668	0.558	0.228	0.127	0.058	0.657	0.668	0.558
0.3	0.229	0.130	0.063	0.657	0.664	0.551	0.229	0.132	0.067	0.657	0.661	0.547
0.5	0.229	0.133	0.074	0.654	0.655	0.538	0.230	0.142	0.087	0.650	0.641	0.524
0.7	0.228	0.137	0.085	0.650	0.645	0.525	0.232	0.162	0.127	0.634	0.608	0.488
0.9	0.226	0.139	0.092	0.645	0.636	0.516	0.231	0.193	0.193	0.618	0.607	0.489
0.95	0.226	0.140	0.093	0.644	0.636	0.515	0.227	0.207	0.226	0.621	0.625	0.499
1.0	0.229	0.178	0.158	0.638	0.601	0.457	→0	→0	→0	→∞	→0	→∞

Table A2
$F_{\sigma,\mathrm{I}}$ and $F_{\sigma,\mathrm{II}}$ at the corner A and B for a cylindrical inclusion when $l_y/l_x = 10$, $\nu_M = \nu_I = 0.3$

G_I/G_M	$F_{\sigma,\mathrm{I}}$ at A			$F_{\sigma,\mathrm{II}}$ at A			$F_{\sigma,\mathrm{I}}$ at B			$F_{\sigma,\mathrm{II}}$ at B		
l_z/d	2	10	100	2	10	100	2	10	100	2	10	100
→0.0	0.223	0.044	0.450	0.701	0.884	1.081	0.223	0.044	0.450	0.701	0.884	1.081
0.1	0.223	0.044	0.456	0.701	0.886	1.087	0.224	0.041	0.459	0.701	0.886	1.087
0.2	0.223	0.044	0.455	0.701	0.886	1.086	0.224	0.041	0.458	0.701	0.885	1.086
0.5	0.223	0.044	0.443	0.701	0.884	1.075	0.224	0.042	0.432	0.700	0.878	1.062
0.8	0.223	0.044	0.407	0.701	0.879	1.040	0.228	0.063	0.256	0.689	0.819	0.907
0.9	0.223	0.044	0.386	0.701	0.877	1.021	0.232	0.123	0.114	0.676	0.779	0.822
0.95	0.223	0.044	0.378	0.701	0.876	1.013	0.233	0.180	0.160	0.678	0.803	0.854
1.0	0.223	0.044	0.407	0.701	0.878	1.040	→0	→0	→0	→∞	→0	→∞

the aspect ratio and elastic modulus ratio of fibers. The conclusions can be made in the following way.

(1) Fiber pullout is modeled as rectangular and cylindrical inclusions in semi-infinite bodies. Then, the problems were analyzed by the application of the body force method coupled with singular integral equation formulation. The boundaries were divided into several intervals, and unknown body force densities were approximated as the product of fundamental densities and power series.

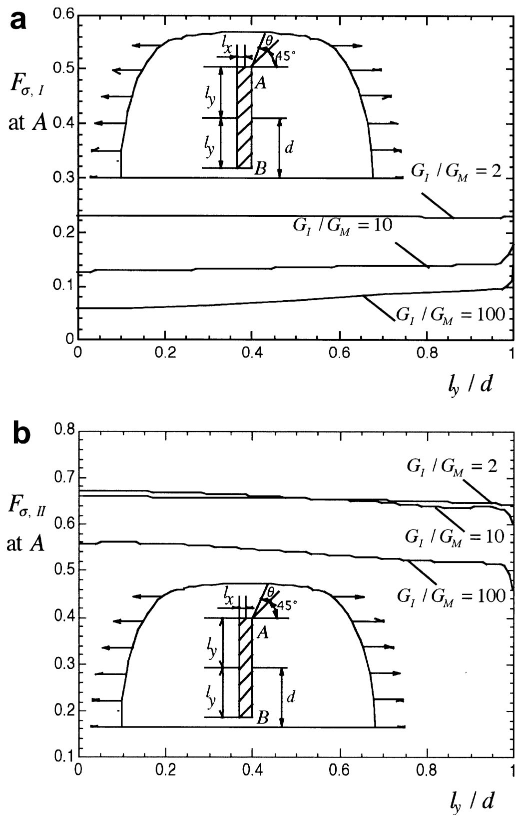

Fig. A3. Stress intensity factors (a) $F_{\sigma,\mathrm{I}}$ (b) $F_{\sigma,\mathrm{II}}$ at A for a rectangular inclusion ($G_I/G_M = 2$, 10, 100, $l_y/l_x = 10$, plane strain, $\nu_M = \nu_I = 0.3$).

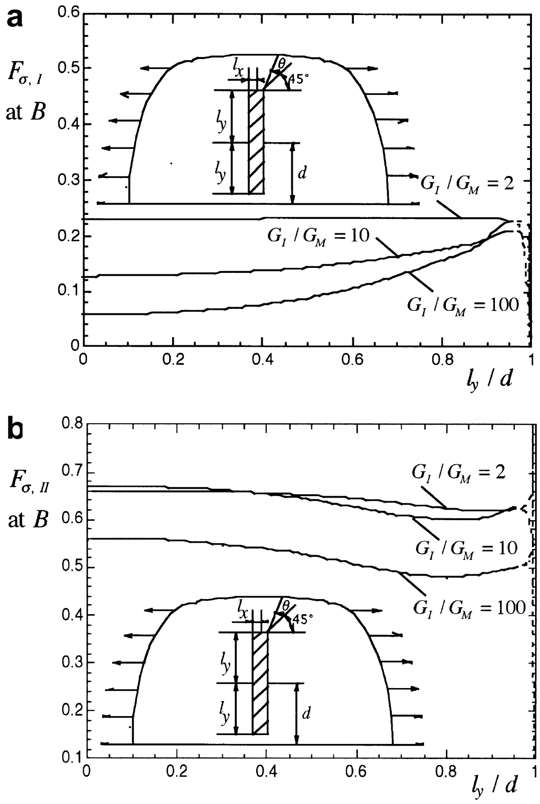

Fig. A4. Stress intensity factors (a) $F_{\sigma,\mathrm{I}}$ (b) $F_{\sigma,\mathrm{II}}$ at B for a rectangular inclusion ($G_I/G_M = 2$, 10, 100, $l_y/l_x = 10$, plane strain, $\nu_M = \nu_I = 0.3$).

The method yields rapidly converging numerical results for generalized stress intensity factors defined at the fiber ends. The results were indicated in tables and figures with varying aspect ratio and elastic modulus ratio of fibers.

(2) For the stress intensity at the fiber end A, the values of $F_{\sigma,\mathrm{I}}$, $F_{\sigma,\mathrm{II}}$ values decrease and approach zero with increasing the fiber aspect ratio l_y/l_x. This can be seen for both rectangular and cylindrical inclusions (see Figs. 8 and 9).

(3) For the stress intensity at the surface end B, the values of F_σ become constant with increasing the fiber aspect ratio l_y/l_x. The values become constant when $l_y/l_x \cong 10$ for both rectangular and cylindrical inclusions independent of elastic modulus ratio G_I/G_M (see Figs. 8 and 9). When the position of pullout force approaches interfacial end, the values of F_σ increase by 1.9 times in the range of $0 \leqslant l/l_x \leqslant 2/3$ (see Fig. 7).

(4) From the results of rectangular inclusion in Fig. 8, the effective length is $l_y/l_x = 4$ for large aspect ratio $l_y/l_x \geqslant 4$. On the other hand, from the results of cylindrical inclusion in Fig. 9, it may be concluded that the effective fiber length is $l_y/l_x = 30$ for large aspect ratio $l_z/l_r \geqslant 30$.

(5) Generalized stress intensity factors $F_\sigma(B)$ at the fiber end at B were compared with the results of bonded strip $F_\sigma(O)$ at O under transverse tension. Then, it is found that the ratio $F_\sigma(B)/F_\sigma(O)$ decreases with increasing l_y/l_x and becomes constant as $l_y/l_x \to \infty$ (see Fig. 6). The value $F_\sigma(O)$ (Chen and Nisitani, 1992) coincides with the present results within 3%.

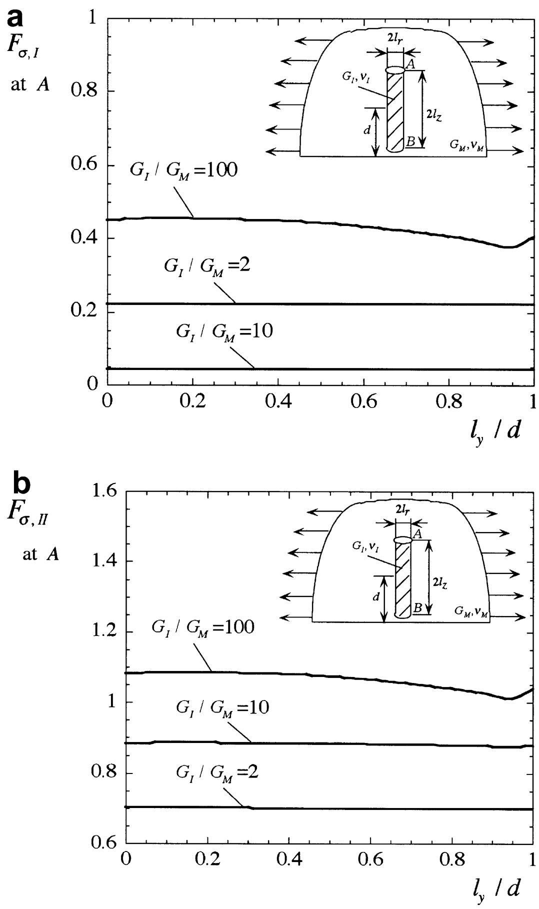

Fig. A5. Stress intensity factors (a) $F_{\sigma,\mathrm{I}}$ (b) $F_{\sigma,\mathrm{II}}$ at A for a cylindrical inclusion ($G_I/G_M = 2$, 10, 100, $l_z/l_r = 10$, $v_M = v_I = 0.3$).

Appendix A. Stress intensity factors for a fiber in a semi-infinite plate under transverse tension

Since structural materials always contain some types of defects such as cracks, cavities, and inclusions, it is necessary to consider the effect on the strength. For example, Fig. A1 indicates the results of a crack in a semi-infinite plate under tension. As shown in Fig. A1, when $l_y/d \to 1$, the stress intensity factor at A becomes larger by 1.586 times, and the stress intensity factor at B becomes infinity. However, if an inclusion exists near free surface, similar results have not been analyzed yet. Therefore, a rectangular inclusion in a semi-infinite plate and a cylindrical inclusion in a semi-infinite body will be treated to evaluate the effect of free surface (see Fig. A2).

Tables A1 and A2 show the results of a rectangular inclusion in Fig. A2 when $l_x/l_y = 1$, 10, $G_I/G_M = 2$, 10, 100. Figs. A3 and A4 show the results of a rectangular inclusion at corners A and B. For corner A, the values of $F_{\sigma,\mathrm{I}}$ and $F_{\sigma,\mathrm{II}}$ do not vary very largely as $l_y/d \to 1$. On the other hand, for corner B, the values of $F_{\sigma,\mathrm{I}}$ and $F_{\sigma,\mathrm{II}}$ should go to infinity or zero depending of G_I/G_M as $l_y/d \to 1$. This is because the singular index becomes different as $l_y/d \to 1$ as shown in Table 3. Similarly, Figs. A5 and A6 indicate the result of a cylindrical inclusion at corner A and B when $l_x/l_y = 10$, $G_I/G_M = 2$, 10, 100.

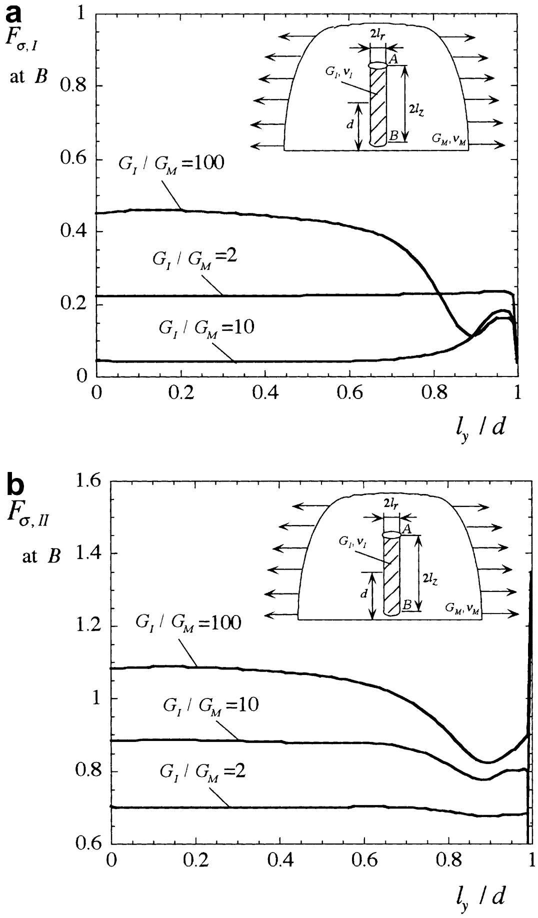

Fig. A6. Stress intensity factors (a) $F_{\sigma,\mathrm{I}}$ (b) $F_{\sigma,\mathrm{II}}$ at B for a cylindrical inclusion ($G_I/G_M = 2$, 10, 100, $l_z/l_r = 10$, $\nu_M = \nu_I = 0.3$).

References

Atkinson, C., Avila, J., Betz, E., Smelser, R.E., 1982. The rod pull out problem, theory and experiment. Journal of the Mechanics and Physics of Solids 30 (3), 97–120.

Budiansky, B., Evans, A.G., Hutchinson, J.W., 1995. Fibre-matrix debonding effects on racking in aligned fibre ceramics composites. International Journal Solids and Structures 32, 315–328.

Chen, D.H., Nisitani, H., 1992. Analysis of intensity of singular stress field at fiber end (2nd report, results of calculation). Transactions of the Japan Society of Mechanical Engineers Series A 58 (555), 143–148 (in Japanese).

Chen, D.H., Nisitani, H., 1993. Intensity of singular stress field near the interface edge point of a bonded strip. Transactions of the Japan Society of Mechanical Engineers Series A 59 (567), 210–214 (in Japanese).

Cook, R.F., Thouless, M.D., Clarke, D.R., Kroll, M.C., 1989. Stick-slip during fibre pull-out. Scripta Metallurgica 23, 1725–1730.

Freund, L.B., 1992. The axial force needed to slide a circular fiber along a hole in an elastic material and implications for fiber pull- Out. European Journal of Mechanics A Solids 11 (1), 1–19.

Luk, V.K., Keer, L.M., 1979. Stress analysis for an elastic half space containing an axially-loaded rigid cylindrical rod. International Journal of Solids and Structures 15 (10), 805–827.

Muki, R., Sternberg, E., 1969. On the diffusion of an axial load from an infinite cylindrical bar embedded in an elastic medium. International Journal of Solids and Structures 5 (6), 587–605.

Muki, R., Sternberg, E., 1970. Elastostatic load-transfer to a half-space from a partially embedded axially loaded rod. International Journal of Solids and Structures 6 (1), 69–90.

Nisitani, H., 1967. The two-dimensional stress problem solved using an electric digital computer. Journal of the Japan Society of Mechanical Engineers 11, 627–632 (in Japanese). [1968. Bulletin of Japan Society of Mechanical Engineers 11, 14–23.].

Nisitani, H., Noguchi, H., Kim, Y.-H., 1993. Fatigue process in short carbon-fiber-reinforced polyamid 6.6 under rotating-bending and torsional fatigue. Engineering Fracture Mechanics 45 (4), 497–512.

Noda, N.A., Kawashima, Y., Moriyama, S., Oda, K., 1996. Interaction of newly defined stress intensity factors for angular corners in a row of diamond-shaped inclusions. International Journal of Fracture 82, 267–295.
Noda, N.A., Matsuo, T., 1998. Singular integral equation method for interaction between elliptical inclusions. ASME Journal of Applied Mechanics 65, 310–319.
Noda, N.A., Moriyama, Y., 2004. Stress concentration of an ellipsoidal inclusion of revolution in a semi-infinite body. Archives of Applied Mechanics 74, 29–44.
Noda, N.A., Takase, Y., 2003. Intensity of singular stress fields at the end of cylindrical inclusion. ASME Journal of Applied Mechanics 70 (4), 487–495.
Noda, N.A., Takase, Y., 2005. Intensity of singular stress at the fiber end in a hexagonal array of fibers. International Journal of Solids and Structures 42 (16–17), 4890–4908.
Noda, N.A., Wang, Q., Uemura, Y., Kawashima, Y., 1998. Singular integral equation method in the analysis of interaction between rectangular inclusions. JSME International Journal Series A 41 (3), 303–308.
Povirk, G.L., Needleman, A., 1993. Finite element simulations of fiber pull-out, transactions of the ASME. Journal of Engineering Materials and Technology 115, 286–291.
Zhang, X., Liu, H.Y., Mai, Y.W., 2004. Effects of fibre debonding and sliding on the fracture behaviour of fibre-reinforced composites. Composites Series A 35, 1313–1323.